

ESR transmission experiments on β' -(ET) $_2\text{SF}_5\text{CF}_2\text{SO}_3$ and (ET) $_2\text{SF}_5\text{NNO}_2$, investigations of spin-Peierls systems.

I.B. Rutel^a, J. Brooks^a, B.H. Ward^b, D. VanDerveer^c, M.E. Sitzmann^d, J. Schlueter^e, R.W. Winter^f, G. Gard^f

^aDepartment of Physics, FSU/NHMFL, 1800 E. Paul Dirac Dr., Tallahassee, FL 32310, USA

^bSchool of Chemistry and Biochemistry, Florida State University, Tallahassee, FL 32310, USA

^cSchool of Chemistry and Biochemistry, Georgia Institute of Technology, Atlanta, GA 30332, USA

^dNaval Surface Warfare Center, Indian Head, MD 20640, USA

^eChemistry and Materials Science, Argonne National Laboratory, Argonne, IL 60439, USA

^fDepartment of Chemistry, Portland State University, Portland, OR 97207, USA

An anisotropic temperature dependent ESR investigation of the organic systems β' -(ET) $_2\text{SF}_5\text{CF}_2\text{SO}_3$ and (ET) $_2\text{SF}_5\text{NNO}_2$ has led to the indication of a spin-Peierls transition at $T_{\text{SP}} = 33$, and 5 K, respectively. We present the details of our investigation and place our data in the context of the general spin-Peierls theory. We also show the dc susceptibility SQUID measurements revealing novel behavior in the second material. Note that to access the high field regime, large fields and high frequencies are needed.

1. Introduction

This paper discusses two organic materials, and the investigation of whether the spin-Peierls transition describes the behavior of each using magnetic resonance techniques. First, a brief description of the characteristics of a spin-Peierls transition will be presented as well as our investigative technique, resonant cavity, and direct transmission ESR. Following the introduction, data collected on the two compounds β' -(ET) $_2\text{SF}_5\text{CF}_2\text{SO}_3$ (CF_2), and (ET) $_2\text{SF}_5\text{NNO}_2$ (NNO_2), (where ET is bis(ethylenedithio)-tetrathiafulvalene) will be presented in the general context of spin-Peierls theory. Crystals of both salts were grown by electrocrystallization methods previously described.¹

The spin-Peierls (SP) transition is a second order magnetic transition that is defined by a structural distortion and subsequent dimerization of the lattice. The transition is best described as a one-dimensional (1D) chain of Heisenberg antiferromagnetic spins that at a given temperature, T_{SP} , progressively dimerize into spin singlet pairs. Consequently, both the anisotropic behavior in the susceptibility is seen, as well as the susceptibility vanishing with decreasing temperature. This is easily distinguished from a three-dimensional (3D)

antiferromagnetic ordering by the decreasing of the susceptibility to zero along all three crystallographic axes in the SP material as opposed to just the easy axis in an antiferromagnetic material.² At temperatures above T_{SP} there are antiferromagnetic fluctuations that indicate the onset of the spin-Peierls transition. Higher temperature behavior is best described by Bonner-Fisher theory (BF), from which the coupling constant, J , can be determined.³

2. Equipment and Techniques

Three techniques were used in characterizing the materials, a cavity resonance transmission technique and a direct transmission technique. The cavity resonance technique was used in conjunction with a Millimeter-wave Vector Network Analyzer (MVNA), with a continually tunable (8-18 GHz) YIG source. Schottky diodes frequency multiply and mix the microwave source to frequencies ranging from 29-220 GHz. These signals then propagate through waveguides to a resonant cylindrical cavity that is 9.55 x 9.31 mm (height x diameter) exciting the fundamental mode (TE_{011}) of 41 GHz^{4, 5}.

The experimental set-up is nearly identical for the direct transmission technique, but allows for measurements, which are impractical with resonant cavities, since the cavity volume decreases inversely with frequency. The probe has the mixer diode replaced with an N_2 cooled detector, a Gunn oscillator multiplies the diode output, and the sample is placed in the waveguide allowing only radiation that passes through the sample to be detected. The resonant cavity is replaced with two 45° mirrors that direct the radiation to the detector.

A dc SQUID measurement was also carried out on the NNO_2 material, using a Quantum Interference Design SQUID, where the field was held at a constant 1 T, and the temperature varied from 350 to 1.7 K.

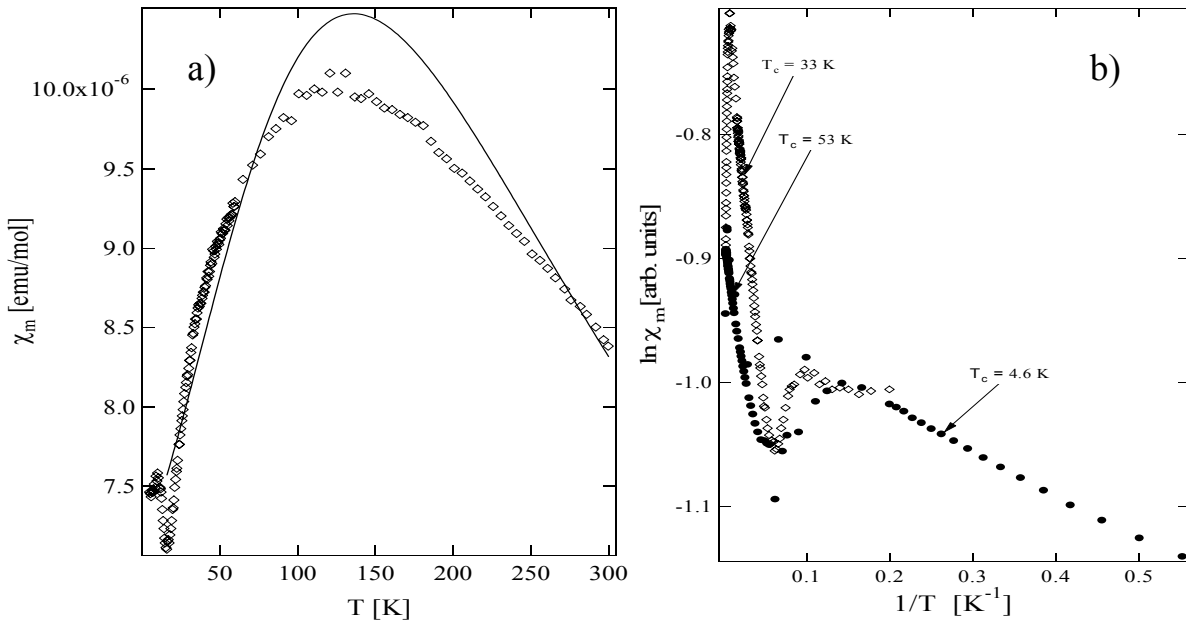


Figure 1: a) SQUID data for the CF_2 (open diamonds) material with the BF fit. b) SQUID data for both samples plotted on an Arrhenius plot, showing the possible onset of two separate transitions, in the NNO_2 sample (filled diamonds) and CF_2 .

3. Results

The β' - $(\text{ET})_2\text{SF}_5\text{CF}_2\text{SO}_3$ is a shiny black rectangular crystal with a β' packing crystal structure. Previous investigation of CF_2 has been performed to determine the nature of the observed magnetic transition at 33K⁴. Previous dc susceptibility measurements, SQUID, indicate the susceptibility vanishes with exponential behavior (Fig 1a). Further investigation was performed in order to determine the characteristics of the transition.

ESR experiments were performed on all three crystallographic directions providing the data in Figure 2.

The runs were performed at 67.57GHz in the resonant cavity configuration, and run over temperatures between 10 and 50 K. For each measurement the sample was mounted with one of the three principle axes parallel to the applied magnetic field, (i.e. $H//a$, $H//b$, and $H//c$). The spectra contain two distinct absorption lines corresponding to the ET and DPPH signals, where the DPPH was used as a marker to calibrate the magnetic field.

The spectra were analyzed by fitting the ESR absorption signal to a Lorentzian line shape and then integrated. The integrated area, which is proportional to the magnetic susceptibility,

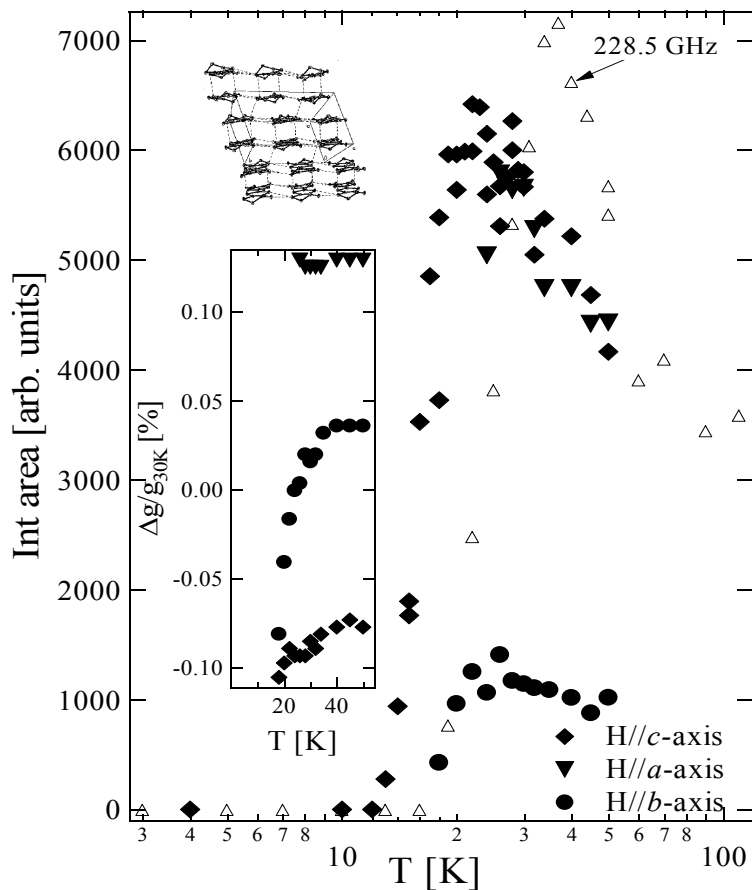


Figure 2: The temperature dependence of the EPR integrated absorption for the resonance line at 67.5 GHz for all three orientations ($H//a$, $H//b$, and $H//c$) for CF_2 . The top inset shows a perspective view of the ET cation layer in the crystal looking down the long axis of the molecule. The dashed lines indicates $\text{S}\cdots\text{S}$ van der Waals contacts less than 3.6 Å. The bottom inset shows the g-shift normalized by the g value at 9 K. The largest change is seen along the b axis showing direct support for the ET molecules being dimerized and forming a 1D chain along the b axis. Symbols are correspond to axis orientation in for both graphs.

is then plotted against temperature in Figure 2. The susceptibility clearly displays a vanishing exponential behavior along all three directions showing the characteristic spin-Peierls behavior. Measurements of both increasing and decreasing temperature show no hysteretic behavior (i.e. 1st order behavior). The activated gap values and relating transition temperatures were found using an exponential function, fit over the transition, ranging from 3 to 33 K⁶. This calculation yields a gap (Δ_σ) and T_{SP} of 114 (± 21) K and 33 (± 7) K respectively, where the uncertainty arises from fitting over slightly different ranges of

temperatures. A BF analysis was also performed in the high temperature regime of the SQUID plot yielding a magnetic exchange constant J_{BF} of 257 K (Fig. 3b).

In the inset of Figure 2, we investigate the

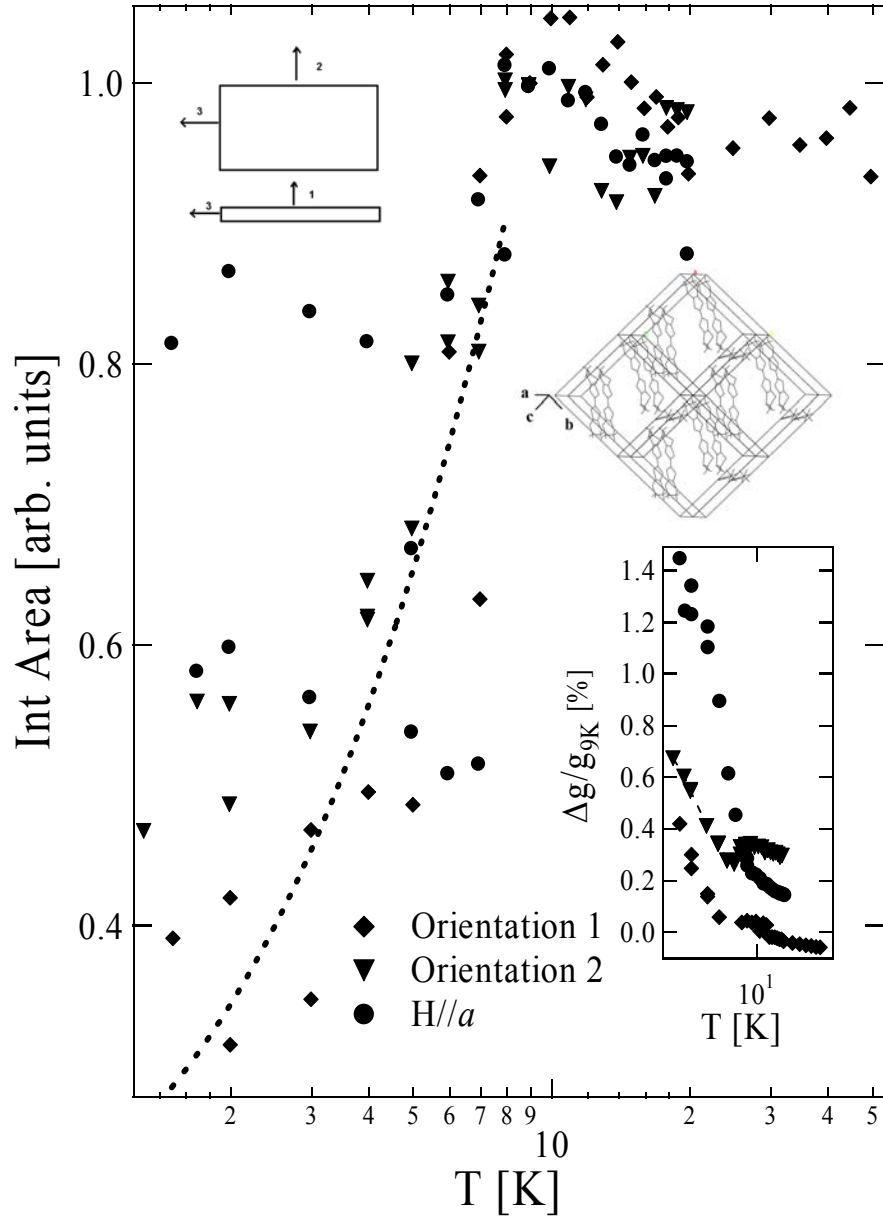


Figure 3: The temperature dependence of the EPR integrated absorption for the resonance line at 79.9 GHz for all three orientations ($H//a$, $H//b$, and $H//c$) for NNO_2 . The dashed line is an exponential fit to the data along orientation 1. The top inset shows the orientation of the sample with respect to the magnetic field (i.e. $H//$ long axis (a) for orientation 3). The second inset is the crystal structure of the NNO_2 material, stacking is along the a axis shown in perspective, into the page. The final inset is the temperature dependent g -shift, where the onset of 3D lattice distortion is evident as a percentage change from the g -value at 30 K, for all 3 directions. Note the feature (dip) in Orientation 2, see text for details.

temperature dependent g -shift of the CF_2 material. The largest change in the g -value occurs along the b -axis ($\sim 0.12\%$), where the b -axis is along the plane (bc) of dimerized ET molecules. The β' crystal packing symmetry results in the initially dimerized ET planes. These ET dimers then undergo the low temperature antiferromagnetic ordering and subsequent singlet ordering consistent with the spin-Peierls transition. This leaves the ET dimers paired with neighboring ET dimers, predominantly in the b direction (some distortion in the a direction is reported by Pigos et al.⁷, evident in the inset by a small change in the a -axis g -shift as well). Overall, the lattice distortions have dimerized quartets of ET molecules, which a detailed X-ray analysis can confirm.⁸

For completeness we now turn to the higher frequency (i.e. field) investigation. The high field runs were carried out using a direct transmission probe with frequencies >220 GHz. By performing experiments at these frequencies we are able to probe the field vs. temperature phase diagram, the high field regime, and the universality of the spin-Peierls transition.

Our experiments were carried out at 228.5 GHz and ~ 11 T. Our data show (open triangles in Fig 2) the transition temperature moving with the increase in field. We have also seen a broadening of the line width with decreasing temperature, which may suggest the onset of a first order transition at 22 K as well, providing evidence of a possible intermediate high field phase.

A similar analysis has been carried out on the $(\text{ET})_2\text{SF}_5\text{NNO}_2$ material⁹, and can be seen in Figure 3. The sample has been placed in a cavity varying the position to line up each crystallographic axis with the magnetic field. This material is a dark brown whisker like crystal with a primitive space group, and preliminary dimensions of 6.52, 15.91, and 15.97 Å for a , b , and c respectively, with angles of 97.2° , 90.3° , and 90.2° for α , β , and γ . A view of the crystal structure is provided in the inset of Figure 3. We are uncertain of the packing symmetry due to the preliminary nature of the crystallography.

The sample was placed in the same cavity from the CF_2 investigation, and the ESR data was collected at a frequency of 79.87 GHz corresponding to a field of 2.54 T, from 1.5 to 50 K. The material shows a precipitous drop in the susceptibility at 8 K. This drop is seen along all three of the principal axes and is confirmed to be second order in nature (from similar hysteresis

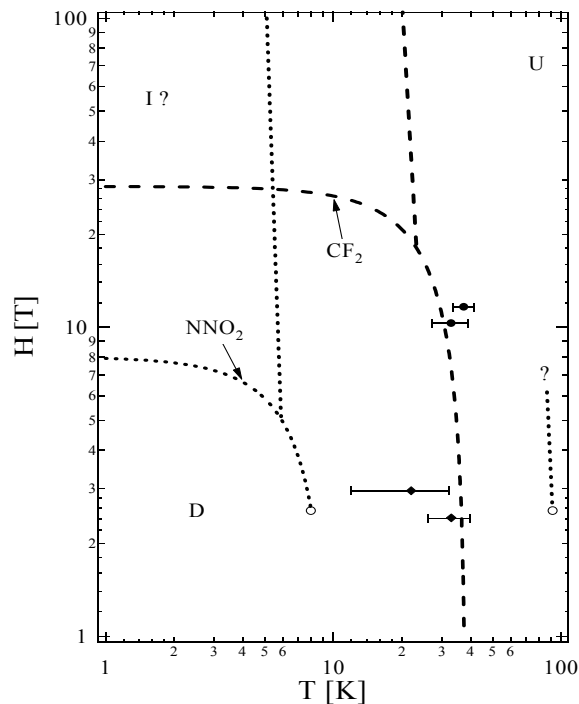


Figure 4: Plot of Phase Diagram for both CF_2 and NNO_2 samples. Universality arguments are introduced with broken lines for both compounds.

arguments as above), but has not been observed to reach zero (as opposed to the CF_2 sample). The signal is weakest when the field is oriented along the stacking direction, a -axis, and when normalized has the largest error, seen in the plot scatter. The transition temperature and gap value of $T_{\text{SP}} = 4.6$ K, and $\Delta_{\sigma} = 8.07$ K respectively, has been calculated using a linear fit on a plot of SQUID data of $\ln \chi_m$ vs. inverse temperature (i.e. an Arrhenius plot) as shown in Figure 1b. A coupling constant of $J_{\text{BF}} = 341$ K was also determined using BF theory, but does not fit well in the high temperature regime.

Analysis of the g -shift shows marked distortion along all principle axes below 8 K. This is consistent with the precursor lattice distortion seen just prior to the onset of the spin-Peierls transition. It appears that the quasi 1D chain axis is not confined to any one of the principle crystal axes. Also of note, is the g -value shift in the second orientation, which distorts in a non-monotonic manner at just above the precursor onset of the transition; suggesting a possible frustration in the lattice from a higher temperature ordered state.

Evidence of this state is seen in the SQUID data (Fig. 2b) which clearly shows a second exponential transition at 53 K. This high temperature order is unexpected, and not seen in the CF_2 material, or other spin-Peierls systems and deserves further investigation.

4. Discussion

A universal phase diagram has been suggested for spin-Peierls materials¹⁰⁻¹³. The two well understood phases are the uniform (U), and Dimerized (D) phases shown in Figure 4. The (U) phase has the spins equidistant, and each spin has equal magnetic coupling (i.e. a single J value). In the Dimerized phase, the spins are distorted and now alternate coupling constants between intra-dimer and inter-dimer interactions.² Guided by previous data presented for compounds like CuGeO_8 , we present Figure 4, and the proposed universality arguments for both compounds described here. The final phase is the (I) phase, and has an intermediate, or incommensurate state. Given a BCS-like transition a general rule for the relationship between critical temperature for $H = 0$, and the critical field for $T = 0$ is approximately $H_c(T=0)/T_{\text{SP}}(H=0) = k_B/\mu_B$ (i.e., the ratio of the Boltzmann constant to the Bohr magneton). We might expect that $H_c(T=0)$ would be of the order 35 and 4 T, for CF_2 and NNO_2 respectively. High field and frequency measurements will be carried out to better understand the universality of both compounds and the nature of the (I) phase itself.

5. Conclusion

Two different materials are presented from the organic class, both showing strong evidence of spin-Peierls behavior. The ESR data show that these materials behave in a Bonner-Fisher like manner in the high temperature regime, which is then followed by an exponential isotropic decrease in the susceptibility with temperature around the transition. We note the details of the crystal structure are not well determined, and that there is a feature in the higher temperature susceptibility. Due to the high temperature of the spin-Peierls transition and the ESR up to 11 T, it seems evident that further high magnetic field ESR will be necessary to compare these materials with others, already studied.

Acknowledgement. Work at NHMFL-FSU was supported by NSF Grant No. DMR-99-71474 and NHMFL/IHRP 500/5031. The NHMFL is supported through a contractual agreement between the NSF through Grant No. NSF-DMR-95-27035 and the State of Florida. Work at Argonne National Laboratory is supported by US-DOE, Office of Basic Energy Sciences, Division of Materials Sciences under contract W-31-109-ENG-38. Research at Portland State University is supported by NSF grant No. CHE-9904316 and the Petroleum Research Fund ACS-PRF 34624-AC7. Thanks also to Sergei Zvyagin and Fivos Drymiotis.

References

- 1 B. H. Ward, J. A. Schlueter, U. Geiser, *et al.*, Chem. Mat. **12**, 343 (2000).
- 2 J. W. Bray, L. V. Interrante, I. S. Jacobs, *et al.*, in *Extended Linear Chain Compounds*, edited by J. S. Miller (Plenum Press, New York, 1982), Vol. 3, p. 353.
- 3 J. C. Bonner and M. E. Fisher, Phys. Rev. **135**, 640 (1964).
- 4 B. H. Ward, I. B. Rutel, J. Brooks, *et al.*, J. Phys. Chem. B **105**, 1750 (2001).
- 5 S. Hill, J. S. Brooks, J. S. Qualls, *et al.*, Physica B **246-247**, 110 (1998).
- 6 A. C. Rose-Innes and E. H. Rhoderick, *Introduction to Superconductivity* (Pergamon Press, New York, 1988).
- 7 J. M. Pigos, B. R. Jones, J. L. Musfeldt, *et al.*, Chemistry of Materials **13**, 1326 (2001).
- 8 J. A. Schlueter, *et al.* to be published .
- 9 B. H. Ward, *et al.* crystal data to be published .
- 10 J. Northby, H. Groenendijk, and L. Jongh, PRB **25**, 3215 (1982).
- 11 V. Kiryukhin, B. Keimer, and D. Moncton, PRL **74**, 1669 (1995).
- 12 U. Ammerahl, T. Lorenz, B. Büchner, *et al.*, Zeitschrift Für Physik **102**, 71 (1997).
- 13 T. Hijmans, H. Brom, and L. Jongh, PRL **54**, 1714 (1985).